GEOLOGICAL JOURNAL
Geol. J. **39**: 157–178 (2004)
Published online 14 May 2004 in Wiley InterScience (www.interscience.wiley.com). DOI: 10.1002/gj.950

Origin, age and petrogenesis of Neoproterozoic composite dikes from the Arabian-Nubian Shield, SW Jordan

G. JARRAR[1], G. SAFFARINI[1], A. BAUMANN[2] and H. WACHENDORF[3]*

[1]*Department of Geology, University of Jordan, Amman, Jordan*
[2]*Institut für Mineralogie, Zentrallaboratorium für Geochronologie, Münster, Germany*
[3]*Institut für Geowissenschaften der TU Braunschweig, Braunschweig, Germany*

The evolution of a Pan-African (*c*. 900–550 Ma) suite of composite dikes, with latite margins and rhyolite interiors, from southwest Jordan is discussed. The dikes cut the Neoproterozoic calc-alkaline granitoids and high-grade metamorphic rocks (*c*. 800–600 Ma) of the northern Arabian-Nubian Shield in Jordan and have been dated by the Rb-Sr isochron method at 566 ± 7 Ma. The symmetrically distributed latite margins constitute less than one-quarter of the whole dike thickness. The rhyolite intruded a median fracture within the latite, while the latter was still hot but completely solidified.

The dikes are alkaline and bimodal in composition with a gap in SiO_2 between 61 and 74 wt%. Both end members display similar chondrite-normalized rare earth element patterns. The rhyolites display the compositional signature of A-type granites. The $(La/Lu)_N$ values are 6.02 and 4.91 for latites and rhyolites, respectively, and the rhyolites show a pronounced negative Eu anomaly, in contrast to the slight negative Eu anomaly of the latites. The chemical variability (e.g. Zr/Y, Zr/Nb, K/Rb) within and between latites and rhyolites does not support a fractional crystallization relationship between the felsic and mafic members of the dikes. We interpret the magma genesis of the composite dikes as the result of intrusion of mantle-derived mafic magma into the lower crust in an extensional tectonic regime. The mafic magma underwent extensive fractional crystallization, which supplied the necessary heat for melting of the lower crust. The products of the initial stages of partial melting (5–10%) mixed with the fractionating mafic magma and gave rise to the latite melts. Further partial melting of the lower crust (up to 30%) produced a felsic melt, which upon 50% fractional crystallization (hornblende 15%, biotite 5%, feldspars 60%, and quartz 20%) gave rise to the rhyolitic magma. Copyright © 2004 John Wiley & Sons, Ltd.

Received 20 March 2002; revised version received 2 March 2003; accepted 20 March 2003

KEY WORDS Jordan; Pan-African Orogeny; Arabian-Nubian Shield; composite dikes; A-type granite; Rb-Sr dating.

1. INTRODUCTION

Composite dikes comprise contrasting contemporaneous mafic and silicic intrusions and occur essentially in two different forms: those with mafic margins and those with silicic margins (e.g. Snyder *et al*. 1997; Wiebe and Ulrich 1997). In any igneous complex only one type is present or at least is dominant. The composite dikes of the Neoproterozoic terrain in south Jordan, in particular, and in the Arabian-Nubian Shield in general, are those with mafic margins. Composite dikes have recently been the subject of numerous research papers, which discussed their mechanism of emplacement as well as the interaction of the two contrasting magmas building these dikes (e.g. Snyder *et al.* 1997; McLeod and Tait 1999; Koyaguchi and Kaneko 1999).

The petrogenesis of granitic rocks in general and the post-orogenic and anorogenic (or A-type) alkaline granites in particular, is still a matter of debate. Three main models have been discussed so far: (1) anatectic crustal melts

* Correspondence to: G. Jarrar, Department of Geology, University of Jordan, Amman, Jordan. E-mail: jarrargh@ju.edu.jo

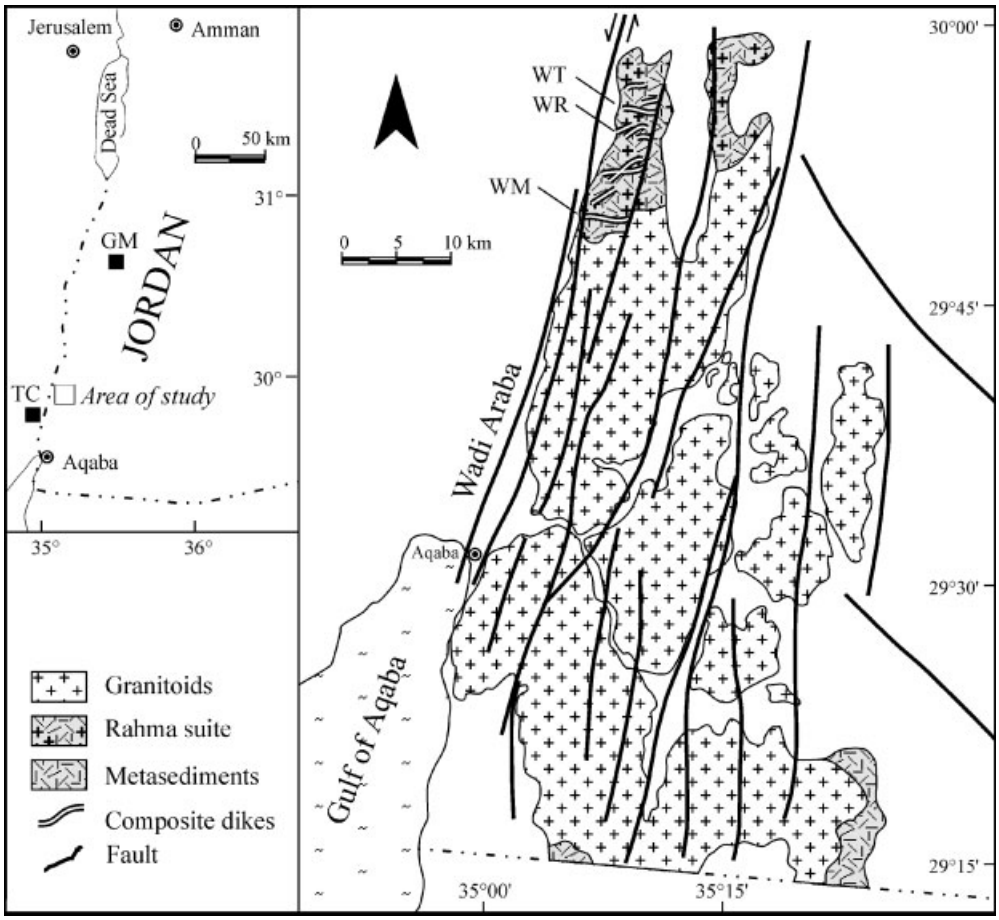

Figure 1. Simplified geological map of the crystalline basement NNE of Aqaba (Jordan) and the location of the composite dikes (WT, Wadi Turban; WR, Wadi Rahma; WM, Wadi Muhtadi); Ghuweir Mafics (GM); and Timna Complex (TC). Modified after Bender (1974) and Ibrahim and McCourt (1995).

(Creaser *et al.* 1991; Landenberger and Collins 1996); (2) fractional crystallization products of mafic magmas (Turner *et al.* 1992; Beyth *et al.* 1994); and (3) as products of silicate liquid immiscibility (Bender *et al.* 1982).

This paper discusses the age, origin, and geodynamic evolution of composite dikes in the Wadi Araba area in SW Jordan (Figure 1) on the basis of field evidence, petrographic, geochemical, and isotopic data. The genetic relationships between latites and rhyolites are explained by fractional crystallization, assimilation and crustal anatexis. The quasi-concurrent emplacement of the latite and rhyolite magmas marks the transition from calc-alkaline to alkaline magmatic activity which follows the tectonic change from orogenic to anorogenic tectonic regime. This paper contributes to: (1) a better understanding of bimodal igneous activity and petrogenesis of A-type granitic magmas; (2) formation of composite dikes; and (3) understanding the magmatic evolution of the final stage of the formation of the Arabian-Nubian Shield (ANS).

2. GEOLOGICAL SETTING

The Pan-African (900–550 Ma; Kröner 1984) basement in SW Jordan, which forms the northernmost exposures of the Arabian-Nubian Shield (Figure 1), is composed of voluminous 625–600 Ma old I-type granitoids (Jarrar 1985) usually emplaced into $\leq$800 Ma mafic and metamorphic rocks (Jarrar 1985, 1998). The final stage (600–550 Ma)

of the Pan-African evolution of the Arabian-Nubian Shield in Jordan and adjacent countries (Jarrar *et al.* 1993) is characterized by the deposition of post-orogenic, intramontane molasse sediments (Jarrar *et al.* 1991) and the emplacement of bimodal, alkaline volcanic to subvolcanic products in an extensional tectonic environment (Jarrar *et al.* 1992; Beyth *et al.* 1994; Garfunkel 1999).

A noticeable feature of the basement in south Jordan is the extensive distribution of subvolcanic dikes (Figure 1) of diverse composition (rhyolite, latite, basalt, lamprophyre). The majority of these dikes consists of a single magma type; however, some dikes are compositionally bimodal, with a rhyolite core flanked by relatively thin latite rims (Wachendorf *et al.* 1985). These dikes are part of the so-called Araba complex (Ibrahim and McCourt 1995), which post-dates the intra-Precambrian unconformity in Jordan and elsewhere in the Arabian-Nubian Shield at about 600 Ma (e.g. Jarrar *et al.* 1993).

Composite dikes of similar age and tectonic setting have been described in other segments of the ANS. Stern and Voegeli (1987) examined the petrogenetic relationship between andesitic and rhyolitic melts in a composite dike in the North Eastern Desert of Egypt. However, the evolution of this dike, and in particular the petrogenesis of the rhyolite core, 'remained enigmatic' in so far as 'the rhyolite formed by fractional crystallization of the andesite or by anatexis of young amphibolite-facies crust' (Stern and Voegeli 1987). The age of a representative NE-trending Pan-African bimodal basalt–rhyolite dike from southern Sinai was determined at 591 ± 9 Ma (Stern and Manton 1987). The hypabyssal rock suite of the Timna Complex (Figure 1) comprises similar composite andesite–rhyolite dikes (Beyth *et al.* 1994). Friz-Töpfer (1991) differentiated three Pan-African dike swarms in southern Sinai. The oldest swarm (*c*. 590 Ma) consists of a bimodal suite of andesites and rhyolites, which display a significant calc-alkaline affinity with a strong Nb-Ta anomaly.

3. FIELD RELATIONSHIPS

The composite dikes under investigation crop out on the eastern shoulder of the Wadi Araba/Dead Sea Transform, about 45 km NNE of Aqaba (Figures 1 and Plate 1a). The dikes intrude the porphyritic granitoids of the Rahma suite (Ibrahim and McCourt 1995), which in turn are hosted by a cordierite-bearing gneiss. The gneiss and the granites have been dated by U-Pb and Rb-Sr methods at 800 Ma and 600 Ma, respectively (Jarrar, unpublished data). They are cut by three generations of dikes: (1) one-metre thick synplutonic microdiorite dikes gently dipping to the NNE (Plate 1a and Figure 2) displaying evidence for magma mingling at their contacts with the host granite, a typical feature for synplutonic dikes (Sha'ban 1996); (2) NE-trending subvertical composite dikes with rhyolite cores and latite rims (Plate 1a and Figure 2); and (3) a younger suite represented by the ENE-trending dolerite dikes dated at 545 ± 13 Ma by the K-Ar method (Jarrar *et al.* 1992; Jarrar 2001) and containing droplets and globules of pyrite.

The composite dikes are about 20 m wide and can be traced for more than 5 km. Generally, the mafic latite rims do not exceed one-quarter of the total thickness of the symmetrical composite dike. On either margin, the thickness of the latite is about 2 m maximum. The thickness of the rhyolite rarely exceeds 15 m. This feature, i.e. the thickness ratios of the mafic and felsic parts of the composite dikes, is typical of composite dikes with mafic margins reported in the literature (e.g. Snyder *et al.* 1997). The dike at Wadi Turban (WT), which has been dated and subjected to detailed sampling, has a local asymmetric distribution of the latite rims due to a younger intrusion of a sulphide-bearing dolerite dike (Figure 2).

Chilling of the latite against the host granite is evident but not intense. By contrast, the rhyolite encloses xenoliths of latite that are elongated and oriented parallel to subparallel to the margins. These are up to 40 cm in greatest dimension and are concentrated on either side of the inner contacts extending inwards for about 2 m (Plate 1c and d). The latite xenoliths prove that the felsic member was emplaced along a median fracture in the latite dike. Furthermore, the rhyolite/latite contacts are knife-sharp and lack signs of chilling. The symmetry of the latite rims implies that the centre of these dikes represent the weak surface along which the rhyolitic melt ascended. On the other hand, the sharp contacts indicate that the latite was solid but still hot at the time of rhyolite intrusion, as evidenced by the lack of rhyolite chilling against latite (Snyder *et al.* 1997).

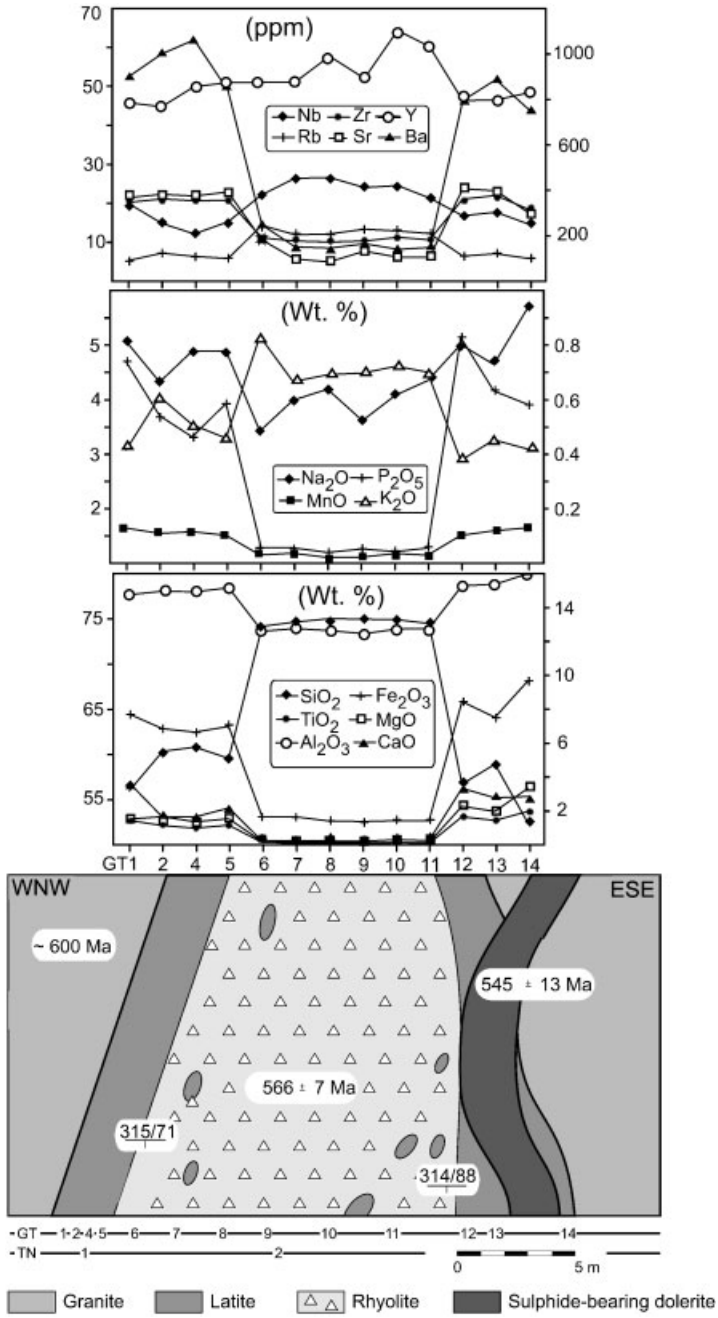

Figure 2. Schematic diagram of the Wadi Turban composite dike, together with sample locations and major and trace elements concentration profiles across the dike.

4. PETROGRAPHY

The fine-grained latite margins of the dikes are greenish-brown and slightly porphyritic. The amount of sericitized plagioclase (andesine) phenocrysts (<3 mm) is less than 5%. The mafic minerals are pyroxenes altered to chlorite.

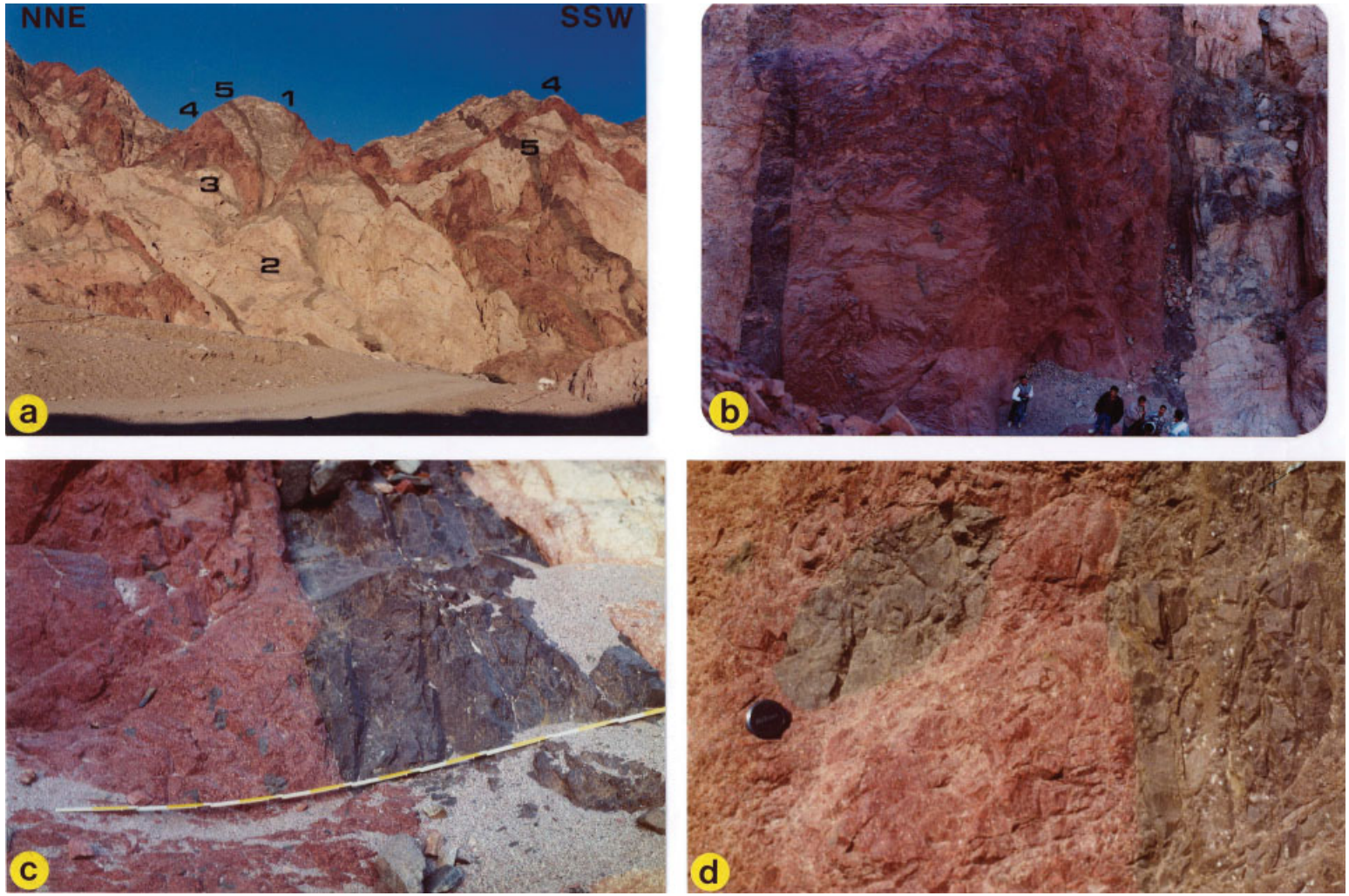

Plate 1. (**a**) Field aspects of the investigated Neoproterozoic dikes in Wadi Araba, SW Jordan: 1, cordierite-bearing gneiss (*c.* 800 Ma); 2, Porphyritic monzogranite (*c.* 600 Ma); the three generations of dikes intruding the Neoproterozoic basement in Wadi Rahma are: 3, synplutonic microdiorite dikes; 4, composite dike (latite rims are not visible); 5, sulphide-bearing dolerite dike (545 ± 13 Ma). (**b**) A typical composite dike with latite rim and rhyolite core (no. 4 in a). (**c**) Knife-sharp latite–rhyolite contact. Rhyolite core with elongated, subparallel arranged latite enclave (scale 2 m). (**d**) Elliptical latite enclave in rhyolite. The diameter of the lens cap is 5.2 cm.

A microcrystalline, trachytic to intergranular groundmass consists of plagioclase and sanidine laths, chloritized pyroxene, actinolitic amphibole, interstitial quartz, and apatite needles. Opaque granules of titanomagnetite are common. One xenolith containing garnet intergrown with calcite was found within the latite. This xenolith might have been sampled from cordierite gneiss among the host rocks. The rhyolite is reddish pink and has a distinctive porphyritic texture, with up to 25% phenocrysts of quartz, sericitized sanidine (<5 mm) and albitic plagioclase. Most phenocrysts are characterized by corrosion embayment and reaction rims, and alkali feldspar phenocrysts are rimmed with overgrowths of albite. The microcrystalline groundmass displays a granophyric texture and consists of intergrown quartz and feldspar with few aegirine grains. Euhedral cubes of fluorite are present. Euhedral amphibole phenocrysts are rare.

5. ANALYTICAL METHODS

Major and trace element data for samples from the composite dike of Wadi Turban were obtained using X-ray fluorescence (XRF) on pressed pellets at the Federal Institute for Geosciences (BGR, Hanover, Germany). The accuracy of the XRF analyses ranges between 1 and 2% for SiO_2 and 2 to 10% for other major oxides and trace elements. The remaining samples were analysed for major, trace and rare earth elements (REE) at the Institut für Geowissenschaften, TU Braunschweig, by inductively coupled plasma atomic emission spectrometry (ICP-AES). The REE were separated using the resin Ag50WX12 sulphonated polystyrene cation exchanger in hydrogen form following the procedure of Zachmann (1988). The accuracy for the ICP-AES method for the major and trace elements ranges between 2 and 7%, and 2 to 10% for the rare earth elements.

The Rb-Sr isotopic analyses were conducted at the Zentrallaboratorium für Geochronologie (ZLG) at the University of Münster, Germany, according to the method described by Blaxland *et al.* (1979). The analytical errors are assigned on the basis of replicate analyses at 1 and 0.1% for $^{87}Rb/^{86}Sr$ and $^{87}Sr/^{86}Sr$, respectively. The decay constants used for the calculations are those recommended by Steiger and Jäger (1977).

6. GEOCHEMISTRY

6.1. Major elements and classification

The geochemical analyses of 29 samples (16 latites, 13 rhyolites) are presented in Table 1. The major elements vary up to 3 wt% within each rock type, except for silica, which shows a wider range of variation in latites (Table 1). In spite of a greater width compared to the latite rims, the rhyolite has a distinctively uniform composition. Approaching the latite/rhyolite interface, a systematic variation of elements was not observed. The distribution of trace elements is comparable with the major element patterns. The variations of major elements and selected trace elements are plotted as a function of distance for the Wadi Turban dike, which was sampled in detail (samples GT 1–14). The compositional bimodality is distinct across the dike in terms of major and trace element geochemistry, with a pronounced symmetrical distribution pattern (Figure 2).

The dikes have SiO_2 contents that range between 51% and 77 wt%, with a compositional gap between 61 and 74 wt%. The samples plot in the fields of basaltic trachyandesite (S2), trachyandesite (S3) and rhyolite (R) on total alkalis versus silica diagram (Figure 3a; Le Bas *et al.* 1986). In a further subdivision of the basaltic trachyandesite and trachyandesite fields on the basis of Na_2O/K_2O (Le Bas *et al.* 1986), these samples plot in the fields of latite (11 samples) and shoshonite (5 samples). Furthermore, the investigated rocks have a predominantly alkaline and high-K character (Figure 3a and b). The alkali nature of the rhyolites is consistent with the presence of aegirine. The distinctive bimodality of the composite dikes is further confirmed by the trace element classification scheme of Winchester and Floyd (1977). The mafic samples plot in the field of andesite and straddle the boundary to rhyodacite/dacite, whereas the rhyolites plot almost exclusively in the rhyolite field (Figure 3c). For the sake of simplicity, the relatively mafic and felsic end members of the dikes will be referred to hereafter as latite and rhyolite, respectively.

Table 1. Chemical composition of the investigated composite dikes. Prefixes GT and TN are for samples from Wadi Turban; prefixes M and RA are for samples from Wadi Rahma

	Latites																Rhyolites												
	GT1	GT2	GT4	GT5	GT12	GT13	GT14	GT15	GT16	GT17	GT20	GT21	M1	RA2	RA3	TN1	GT6	GT7	GT8	GT9	GT10	GT11	GT22	GT23	GT24	M2	RA4	RA5	TN2
SiO_2	60.48	60.64	61.14	59.73	56.64	58.94	52.55	60.17	53.06	58.95	57.92	55.94	51.9	56.14	54.17	58.96	74.34	74.86	74.99	75.12	74.95	74.73	74.81	75.04	74.81	76.92	76.87	75.84	75.04
TiO_2	1.61	1.3	1.18	1.34	1.73	1.43	1.92	1.34	1.99	1.39	1.57	1.74	1.13	1.08	1.12	1.08	0.18	0.18	0.12	0.14	0.12	0.15	0.17	0.13	0.18	0.07	0.08	0.21	0.16
Al_2O_3	14.87	15.13	14.99	15.29	15.14	15.31	15.84	14.64	16.09	14.73	15.01	15.26	15.84	14.44	14.78	14.72	12.71	12.8	12.7	12.51	12.73	12.78	12.74	12.57	12.6	12.04	12.61	11.98	12.81
Fe_2O_3	2.36	2.1	2.04	2.16	2.57	2.25	2.9	2.07	2.71	2.18	2.32	2.56	3.41	2.99	2.73	2.66	0.51	0.52	0.45	0.44	0.44	0.46	0.48	0.44	0.51	0.4	0.4	0.58	0.51
FeO	4.94	4.4	4.28	4.53	5.4	4.72	6.1	4.35	5.69	4.57	4.87	5.37	7.17	6.29	5.74	5.59	1.06	1.09	0.94	0.92	0.91	0.96	1.01	0.93	1.08	0.84	0.84	1.22	1.06
MnO	0.13	0.1	0.11	0.1	0.1	0.12	0.13	0.1	0.15	0.14	0.14	0.15	0.2	0.16	0.16	0.1	0.03	0.04	0.03	0.03	0.04	0.03	0.04	0.03	0.03	0.02	0.02	0.04	0.04
MgO	1.72	1.79	1.51	1.68	2.27	2.01	3.32	2.52	4.01	2.97	2.12	2.31	5.18	5.2	4.86	2.22	0.2	0.18	0.11	0.14	0.11	0.15	0.17	0.11	0.11	0.14	0.17	0.5	0.29
CaO	3.82	1.78	1.82	2.3	3.33	2.79	2.86	2.58	3.59	2.55	3.22	3.33	5.43	3.71	3.19	3.95	0.31	0.28	0.24	0.25	0.25	0.25	0.29	0.19	0.28	0.5	0.13	0.58	0.34
Na_2O	5.08	4.35	4.85	4.84	5.01	4.67	5.71	4.79	5.4	4.84	4.68	5.68	3.47	4.63	5.17	5.64	3.45	4.00	4.21	3.7	4.11	4.35	4.06	4.61	4.14	3.56	3.93	3.5	3.97
K_2O	3.09	4.07	3.55	3.31	2.89	3.28	3.06	2.23	0.65	2.15	3.11	2.78	2.4	1.52	2.52	2.46	5.17	4.3	4.48	4.95	4.64	4.5	4.49	4.3	4.49	4.84	5.34	4.9	4.97
P_2O_5	0.74	0.55	0.48	0.59	0.83	0.64	0.59	0.41	0.57	0.41	0.74	0.82	nd	nd	nd	nd	0.06	0.06	0.03	0.05	0.04	0.05	0.06	0.04	0.06	nd	nd	nd	nd
LOI	3.94	2.7	2.73	2.93	2.83	2.79	3.63	3.8	4.95	3.98	3.29	2.95	2.83	4.36	4.35	2.84	1.19	1.11	1.08	1.04	0.98	1.03	0.95	0.93	1.14	0.62	0.49	0.85	0.57
SUM	98.78	98.91	98.67	98.8	98.75	98.94	98.66	99.00	98.87	98.85	98.99	98.89	98.96	100.5	98.79	100.2	99.21	99.42	99.38	99.29	99.32	99.44	99.28	99.32	99.43	99.95	100.9	100.2	99.76
Trace elements and elemental ratios																													
Cr	<15	<15	<15	<15	<15	<15	19	<15	<15	17	<15	<15	31	28	26	9	<15	<15	<15	<15	<15	<15	<15	<15	<15	5	4	5	7
Ni	<5	<5	<5	<5	<5	<5	7	9	7	8	<5	<5	17	13	16	5	<5	<5	<5	<5	<5	<5	<5	<5	<5	4	1	5	4
Sc	19	17	18	19	21	18	23	14	25	16	19	23	20	21	22	18	<2	<2	3	<2	3	<2	<2	3	4	2	2	3	3
V	151	95	91	110	166	119	174	132	185	154	162	159	185	188	191	171	17	23	21	<15	<15	16	23	<15	15	6	4	17	12
Cu	15	13	17	11	9	10	15	24	55	14	15	13	13	12	15	10	7	<7	14	11	<7	13	<7	9	16	3	3	8	3
Zn	112	109	109	102	133	110	184	210	204	144	144	157	144	168	411	132	45	56	42	94	52	46	50	44	53	53	68	74	54
Rb	92	123	110	102	104	114	91	105	37	104	93	89	166	55	26	70	238	205	195	227	217	201	187	171	188	210	181	197	236
Ba	906	997	1066	841	789	882	747	188	35	185	915	743	529	355	87	631	251	147	139	157	135	142	21	211	200	126	189	196	160
Sr	369	386	375	389	402	388	282	263	291	355	363	351	526	230	250	308	178	94	84	125	101	104	126	98	84	35	82	108	133
Nb	20	15	12	15	16	17	14	22	13	16	16	20	13	14	17	13	22	26	26	24	24	21	25	26	23	22	25	22	27
Zr	350	359	353	358	354	367	301	253	278	245	352	359	252	308	323	377	186	177	168	171	185	176	181	168	180	144	175	178	185
Y	46	45	50	51	46	46	48	63	70	61	45	49	36	39	60	37	51	51	57	52	64	60	56	58	61	32	41	45	46
Th	<5	5	<5	14	8	14	11	10	<5	7	10	<5	nd	nd	nd	nd	15	13	15	19	26	23	19	12	13	nd	nd	nd	nd
U	<5	<5	<5	5	<5	6	<5	6	<5	7	<5	<5	nd	nd	nd	nd	7	<5	<5	<5	7	8	<5	7	9	nd	nd	nd	nd
La	48	42	26	23	39	28	24	25	36	38	40	39	30	31	nd	47	<20	<20	<20	<20	<20	<20	<20	<20	<20	52	21	nd	25
Ce	96	90	95	101	107	130	63	74	64	38	85	126	70	75	nd	112	52	40	55	38	53	60	50	61	59	121	52	nd	59
K/Rb	279	275	268	269	231	239	279	176	146	172	278	259	120	229	805	292	180	174	191	181	178	186	199	209	198	191	245	206	175
K/Ba	28	34	28	33	30	31	34	98	154	96	28	31	38	36	240	32	171	243	268	262	285	263	177	169	186	319	235	208	258
Rb/Sr	0.25	0.32	0.29	0.26	0.26	0.29	0.32	0.4	0.13	0.29	0.26	0.25	0.31	0.24	0.1	0.23	1.34	2.18	2.32	1.82	2.15	1.93	1.48	1.74	2.24	6	2.21	1.82	1.77
Ba/Zr	2.59	2.78	3.02	2.35	2.23	2.4	2.48	0.74	0.13	0.76	2.6	2.07	2.1	1.15	0.27	1.67	1.35	0.83	0.83	0.92	0.73	0.81	1.16	1.26	1.11	0.88	1.08	1.1	0.86
Y/Nb	2.3	3	4.17	3.4	2.88	2.71	3.43	2.86	5.38	3.81	2.81	2.45	2.77	2.79	3.53	2.85	2.32	1.96	2.19	2.17	2.67	2.86	2.24	2.23	2.65	1.45	1.64	2.05	1.7
Zr/Nb	17.15	23.93	29.42	23.87	22.13	21.59	21.5	11.5	21.38	15.31	22	17.95	19.38	22	19	29	8.45	6.81	6.46	7.13	7.71	8.38	7.24	6.46	7.83	6.55	7	8.09	6.85
Zr/Y	7.61	7.98	7.06	7.02	7.7	7.98	6.27	4.02	3.97	4.02	7.82	7.33	7	7.9	5.38	10.19	3.65	3.47	2.95	3.29	2.89	2.93	3.23	2.9	2.95	4.5	4.27	3.96	4.02
Ce/Nb	4.8	6	7.92	6.73	6.69	7.65	4.5	3.36	4.92	2.38	5.31	6.3	5.38	5.38		8.58	2.36	1.54	2.12	1.58	2.21	2.86	2	2.35	2.57	5.5	2.08		2.22

nd = not determined. The element concentrations with the < sign distinguish analyses carried out with XRF.

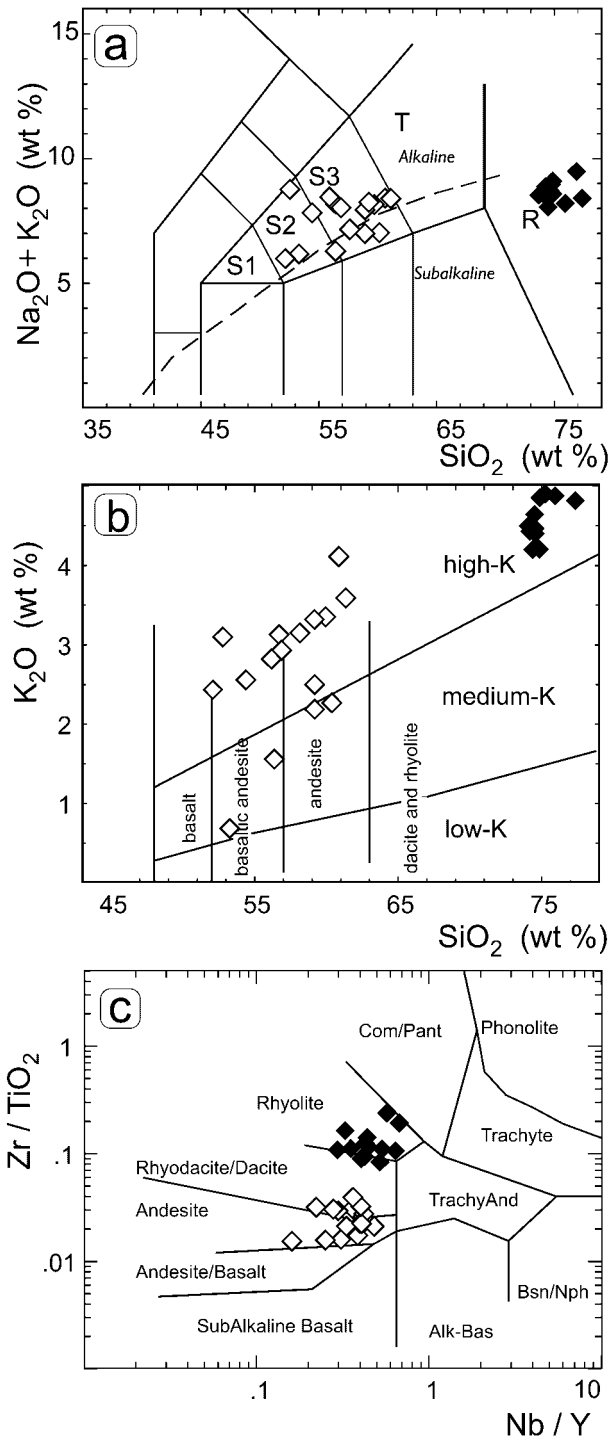

Figure 3. Classification diagrams of the investigated dikes. Open symbols: latites; closed symbols: rhyolites. (**a**) Total alkalis–silica classification diagram after Le Bas *et al.* (1986). The dividing line between alkaline and subalkaline fields are after Irvine and Baragar (1971). (**b**) Variation of K_2O versus SiO_2 showing the medium- and high-K character of composite dikes (after Peccerillo and Taylor 1976). (**c**) Log (Nb/Y) versus log (Zr/TiO_2) diagram after Winchester and Floyd (1977).

The K_2O–silica diagram (Figure 3b) reveals K_2O-enriched nature of the latites and the rhyolites, as manifested by the different values of K_2O enrichment at a constant SiO_2 in latites. Meen (1990) explained the occurrence of magmas showing different levels of K_2O enrichment at constant SiO_2 by high-pressure crystallization. Alternatively, Cribb and Barton (1996) have demonstrated that combined assimilation, fractional crystallization, and mixing (AFM) could generate basaltic trachyandesite and trachyandesites having the type of K_2O enrichment observed in the investigated latites, i.e. different K_2O levels at constant SiO_2. The samples falling in the field of medium-K latites (Figure 3b) represent the melts least affected by the AFM processes.

In contrast to the host granitoids (Abdullah 1989) the rhyolites are characterized by relatively high alkali contents ($> 8\%$ $Na_2O + K_2O$), $CaO < 0.5\%$, and high FeO_{tot}/MgO ($> 8\%$). These chemical signatures are diagnostic of A-type magmas (e.g. Eby 1992). Likewise, the Y/Nb ratio (1.45–2.65; av. 2.16) of the rhyolites is typical of A-type granites (Whalen *et al*. 1987). Yet, the zirconium content of the rhyolites is lower than typical A-type magmas. White *et al.* (1982) suggested that Zr, Nb and Ga form alkali-rich complex ions in fluorine-rich magmas, thus suppressing the saturation of phases such as zircon, which would explain the depletion of zirconium in the investigated rhyolite dikes. Progressive differentiation of the rhyolitic magmas produced Zr-enriched rhyolite flows elsewhere in the region (Jarrar 1992). No fluorine analysis was carried out, but the presence of fluorite in one of the thin-sections indicates the fluorine-rich nature of the rhyolitic magmas.

6.2. Trace and rare earth elements

Figure 4 includes Harker-type variation diagrams of selected element pairs and elemental ratios. These plots reveal the following geochemical features:

- The latites show greater scatter than the rhyolites in almost all binary plots, suggestive of more than one evolutionary trend.
- Both latites and rhyolites cluster with almost no overlap.
- The bimodal distribution of data points in the elemental ratio plots is obvious. The elemental Zr/Nb, Zr/Y and Y/Nb values for the rhyolites are completely different from those for latites. Because fractional crystallization of a latite–rhyolite suite in a closed system should result in constant ratios, the different ratios of latites and rhyolites argue against a fractionation relationship between the two end members.

Vectors of fractional crystallization for pyroxenes, feldspars, biotite, and amphibole have been constructed for mafic and felsic compositions using the equation of Rayleigh fractionation:

$$C_l^i = C_o^i f^{(D^i - 1)}$$

(Arth 1976), where C_o^i is the concentration of the element i in the original melt (the least differentiated sample for each suite, i.e. the latite and rhyolite), C_l^i is the concentration of the element in the melt (daughter) and D^i is the bulk distribution coefficient for element i. The length of the vectors corresponds to calculated concentration taking f-values (fraction of the remaining melt) between 0.7 and 0.5, and the bulk distribution coefficients (Kd's) were calculated from mineral D^i values. The compilation of distribution coefficients for mafic and felsic compositions given by Rollinson (1993) was used in the calculations.

The elemental and element ratio variations in the rhyolites can be explained by fractionation of the mineral assemblage (plagioclase + K-feldspar + quartz) and amphibole and biotite. The phenocryst assemblage in the rhyolite consists exclusively of alkali feldspar, albite plagioclase, and quartz. A relict of one hornblende phenocryst was observed, but no biotite. Hence, the fractionation of these two minerals, i.e. hornblende and biotite, could have taken place early in the evolution of the rhyolite magma. The early fractionation of hornblende is possibly responsible for depleting the rhyolites in zirconium ($Kd^{Zr}_{\text{Hbl-rhyolitic melt}} = 4$; Arth 1976). In contrast to the rhyolite, the mineral vectors calculated for the latites indicate the importance of pyroxene fractionation of (particularly) clinopyroxene, along with plagioclase, hornblende, and biotite. However, fractionation of these minerals cannot

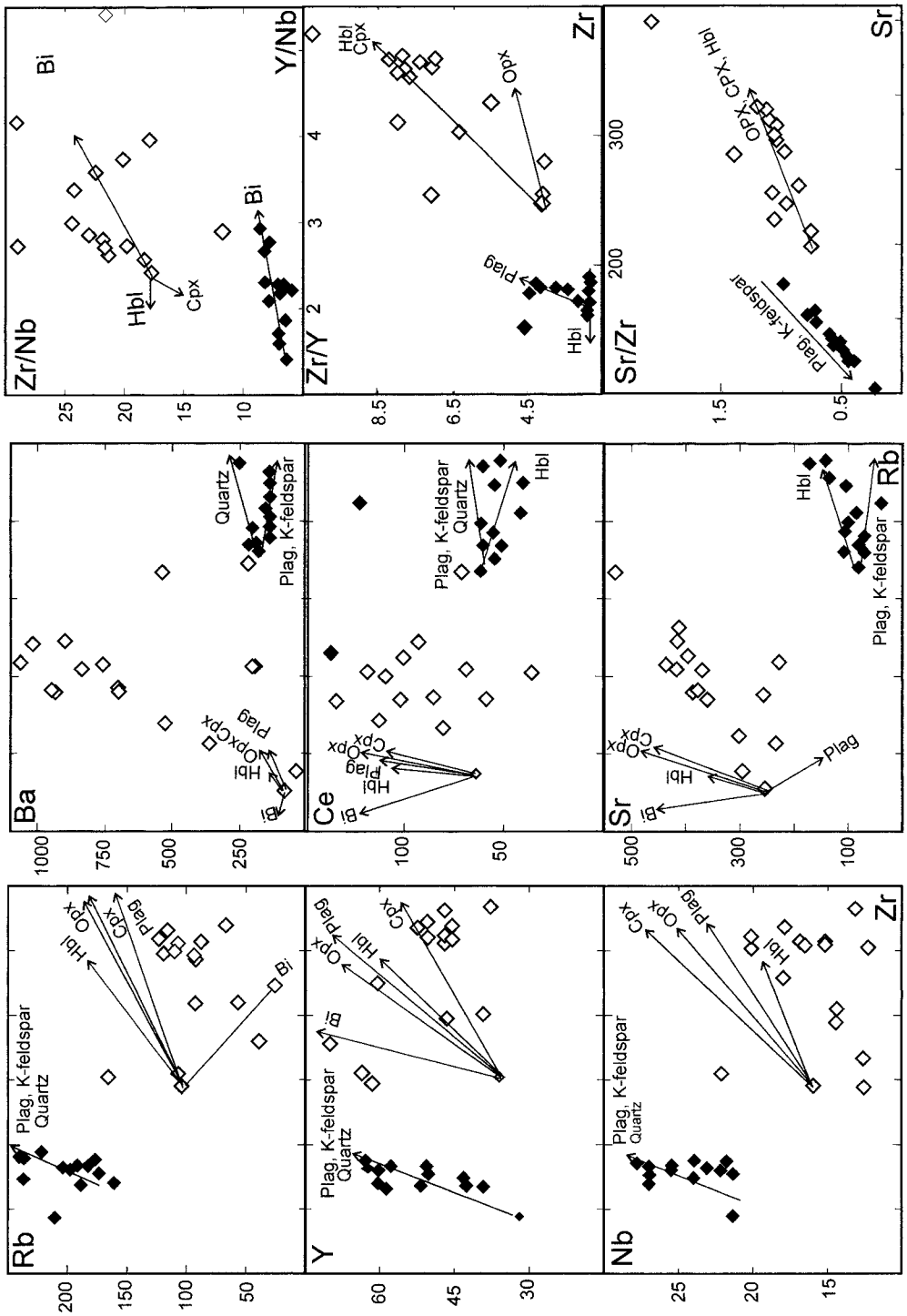

Figure 4. Variation diagrams on binary plots of selected elements and elemental ratios. The modelled mineral fractionation vectors for latites and rhyolites are shown. Symbols as in Figure 3.

explain the bulk chemical variation in the latites. This requires the involvement of another mechanism; assimilation and mixing with rhyolitic magma is discussed in the section on petrogenesis. Furthermore, latites have only a few phenocrysts of andesine and presumable clinopyroxene (altered to chlorite). The latite from Al-Muhtadi composite dike contains fresh clinopyroxene phenocrysts but some were partially altered to chlorite (Wachendorf *et al.* 1985). Accordingly, fractionation of these phases, i.e. plagioclase and clinopyroxene, must have taken place early in the latite magma evolution. The importance of clinopyroxene fractionation is also evident from the negative trend of (CaO/Al_2O_3) versus SiO_2 (diagram not shown).

Grove and Donnelly-Nolan (1986) attributed the compositional gaps in comagmatic fractionated suites to shallow temperature–composition slopes for liquidus surfaces, which allow for large degrees of crystallization and compositional change over a small temperature interval. However, this does not hold for the investigated dikes because both the mafic and felsic magma show not only discontinuous but opposite trends from those expected for fractional crystallization (e.g. Zr/Nb versus Y/Nb, Y versus Zr; Figure 4).

The latites, rhyolites and average A-type granites (Whalen *et al.* 1987) are plotted on an elemental compatibility diagram (Figure 5a). The latites display slight negative Ti, Sr, and Nb anomalies. On the other hand, the rhyolites show strong negative anomalies at Ti, P, Sr, Ba and a slight negative Nb anomaly—patterns similar to A-type granites. The Nb anomaly in the latites is explained as reflecting crustal involvement in their genesis (Rollinson 1993).

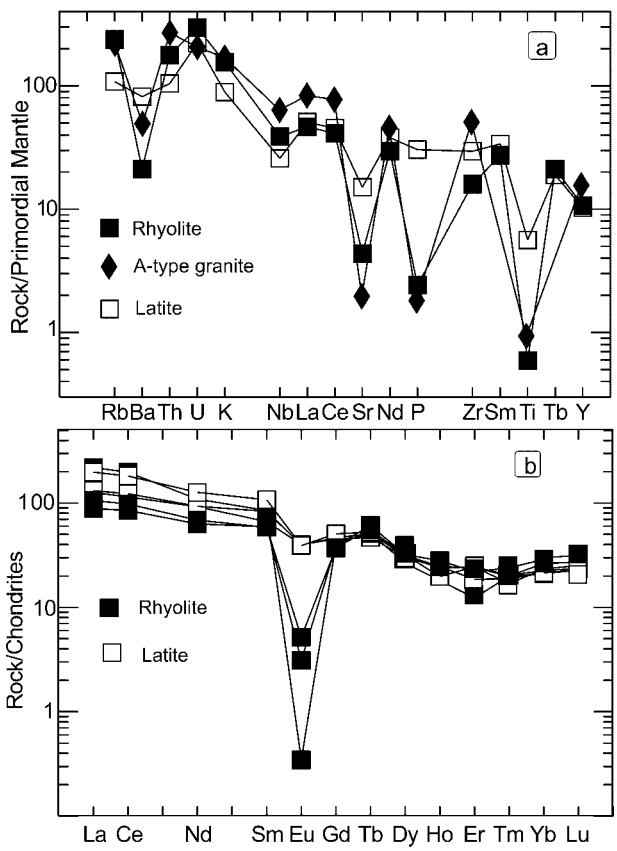

Figure 5. (**a**) Elemental compatibility plot for mean compositions of the studied latite, rhyolite, and A-type granites (Whalen *et al*. 1987). Normalizing values are after Wood *et al*. (1979). (**b**) REE chondrite-normalized plots for the investigated latites and rhyolites. Normalizing values are from Rollinson (1993).

The latites and rhyolites have an average content of REE of 215 ppm and 186 ppm, respectively. The $(La/Lu)_N$ ratio for latites and rhyolites is 6.02 and 4.91, respectively. The rhyolites show a pronounced negative Eu-anomaly ($Eu/Eu^* = 0.13–0.009$), in comparison with the weak negative Eu-anomaly of the latites ($Eu/Eu^* = 0.67–0.80$) (Figure 5b). Barium, Sr, Ti, Y, Nb and Zr decrease in abundance with increasingly negative Eu-anomaly. In contrast, Sr and Rb display an increasing trend emphasizing the importance of feldspar fractionation.

7. TECTONIC SETTING

The emplacement of the composite dikes took place during the final stage of crustal evolution of the Arabian-Nubian Shield in overthickened continental crust. At this stage, the crust was undergoing isostatic adjustment associated with denudation (Dewey 1988), the surface expression of which is in deposition of molasse-type sediments in rift-bounded basins (Saramuj Conglomerate in Jordan (Jarrar *et al.* 1991, 1993), Hammamat series in the North Eastern Desert of Egypt (Akaad and Noweir 1980; Willis *et al.* 1988). The intrusion of these dikes and many others in the ANS (Wachendorf *et al.* 1985; Friz-Töpfer 1991; Pudlo and Franz 1994; Kessel *et al.* 1998) is a manifestation of this extensional tectonic regime. Greiling *et al.* (1994) concluded that the Pan-African orogenic collision in Egypt ended at 615–600 Ma, followed by a subsequent extensional collapse within the time span 595–575 Ma.

The rhyolites plot (with minor overlap) in the within-plate granite (WPG) field on the Nb versus Y and in the field for post-collisional granite on Rb versus (Y + Nb) tectonic discrimination diagrams (Figure 6a and b) of Pearce *et al.* (1984) and Pearce (1996). Granites formed in association with major rifting clearly have a within-plate granite (WPG) affinity and are most likely to be correctly classified based on geochemistry alone (Förster *et al.* 1997). By contrast, extensional granitoids associated with convergent plate boundaries may fall within WPG and volcanic arc granites (VAG), and, in rare cases, even in the collisional granites (COLG) fields on the Rb versus (Nb + Y) plot (Förster *et al.* 1997).

The rhyolites plot exclusively in the field A2 of Eby (1992) of post-orogenic subduction-related A-type granites on the ternary (Nb–Y–Ce) and binary (Rb/Nb versus Y/Nb) plots (Figures 6c and d). Eby (1992) pointed out that the A2 group represent crust-derived magmas of post-orogenic setting. The latites fall exclusively in the field of within-plate lavas and basalts on the TiO_2 versus Zr (Pearce 1980) and Zr/Y versus Zr (Pearce and Norry 1979) tectonic discrimination diagrams (Figures 6e and f). On the basis of the geochemical and regional tectonic consideration, we place the emplacement of the composite dikes in a post-collisional tectonic regime.

8. AGE RELATIONSHIPS AND RB-SR ISOTOPIC SYSTEMATICS

The Rb-Sr isotopic data for five latites, four rhyolites and one sanidine are listed in Table 2 and plotted in Figure 7. The isotopic variations in rhyolites plot along a best-fit line (not shown) corresponding to an age of 564.4 ± 49 Ma ($Sr_i = 0.703975 \pm 0.0038$; MSWD = 0.64). On the other hand, the data points of the five latites define an isochron, which yields an age of 534 ± 120 Ma ($Sr_i = 0.704162 \pm 0.0011$; MSWD = 0.03). The average age obtained for the latites is too young, as field contact relationships with the rhyolite suggest that latites should be either of the same age or even slightly older than the latites. Even if the latites were considerably older than the rhyolites, the intrusion of the thick rhyolite core just in the middle of the thin latites could have reset the isotopic clock in the latites. Consequently, the data points of both rock types should define two parallel isochrons, i.e equal age. The initial ratios obtained from the two isochrons are similar within the quoted errors. On the basis of this argument and the genetic relationships between the two rock types, we tried to fit the data to a composite isochron of the latites and rhyolites, which yielded an age of 565.6 ± 7 Ma ($Sr_i = 0.703881 \pm 0.00035$; MSWD = 0.99). This is indistinguishable from the age of the rhyolite. We consider this to be the age of the composite dikes in south Jordan. This conclusion is supported by various lines of evidence. The investigated dikes are hosted by a calc-alkaline granite, which has a Rb-Sr whole-rock biotite age of 600 Ma (Brook *et al.* 1990; Jarrar, unpublished data). These granites are intruded by gently dipping synplutonic microdiorite dikes (Sha'ban 1996), which are presumably time

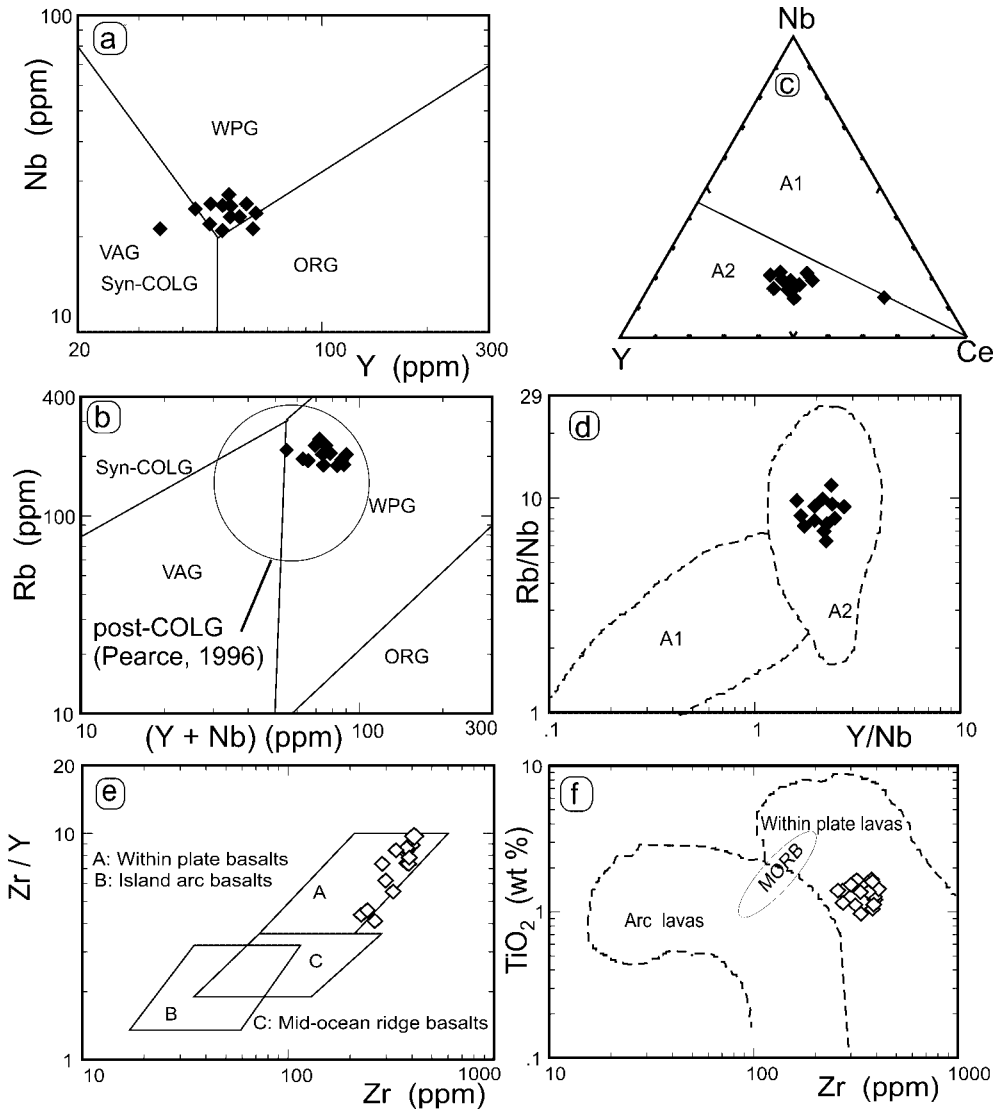

Figure 6. Tectonic discrimination and granite classification diagrams. (**a**) Nb versus Y plot, and (**b**) Rb versus (Y + Nb) plot, both after Pearce *et al*. (1984). WPG, within-plate granite; VAG, volcanic arc granites; ORG, ocean-ridge granite; Syn-COLG, syncollisional granites. The field of post-collisional granites after Pearce (1996). (**c**) Nb–Y–Ce plot, and (**d**) Rb/Nb versus Y/Nb plot, both after Eby (1992). A1, anorogenic A-type granite; A2, subduction-related A-type granites. (**e**) Log Zr/Y versus log Zr tectonic discrimination plot for the latites (Pearce and Norry 1979). (**f**) Log TiO_2 versus log Zr tectonic environment discrimination diagram for the latites (Pearce 1980).

equivalent to the Muhtadi quartz diorites exposed a few kilometres south of Wadi Rahma. The Muhtadi diorites were dated by Rb-Sr whole-rock method at 584 ± 18 Ma (Brook *et al.* 1990). Furthermore, these diorites are intruded by the composite dikes (Wachendorf *et al.* 1985, which are cut by a sulphide-bearing dolerite dated by K-Ar method at 545 Ma (Jarrar *et al.* 1992). The latter dikes have also been dated in Timna by K-Ar and Ar-Ar methods at 546 and 532 Ma, respectively (Beyth and Heimann 1999). The Humrat granite, which is chemically similar to the investigated rhyolites, has been dated at 567 ± 5 Ma by the Rb-Sr method (Brook *et al.* 1990). Moreover, the Ghuweir Mafics in the Feinan area (about 90 km north of the study area; Figure 1) are the rocks most

Table 2. Rb/Sr data of the composite dikes

Sample	Rb (ppm)	Sr (ppm)	$^{87}Rb/^{86}Sr$	$^{87}Sr/^{86}Sr$
Latites				
GT-1	107.6	423.8	0.7348	0.709749
GT-2	115.1	396.5	0.8402	0.710567
TN-1	69.4	307.9	0.6527	0.709115
RA-2	55.5	230.2	0.6977	0.70950
RA-3	26.36	249.6	0.3056	0.706493
Rhyolites				
GT-6	222.3	139.3	4.632	0.741408
GT-7	219.9	138.5	4.609	0.741597
TN-2	236.3	132.8	5.166	0.74454
RA-5	195.6	107.9	5.292	0.746706
RA-8 SAN	433.6	161.3	7.825	0.767119

closely related to the latites and have been dated by the Rb-Sr method at 572 ± 48 Ma ($Sr_i = 0.7036 \pm 0.0005$; Jarrar *et al*. in press). The ages of the composite dikes and the sulphide-bearing dikes are in the same range as those compositionally equivalent dikes and alkaline ring complexes of the North Eastern Desert of Egypt (Stern and Voegeli 1987; Frisch and Abdel-Rahman 1999) and of the Timna Valley (Beyth *et al.* 1994; Beyth and Heimann 1999).

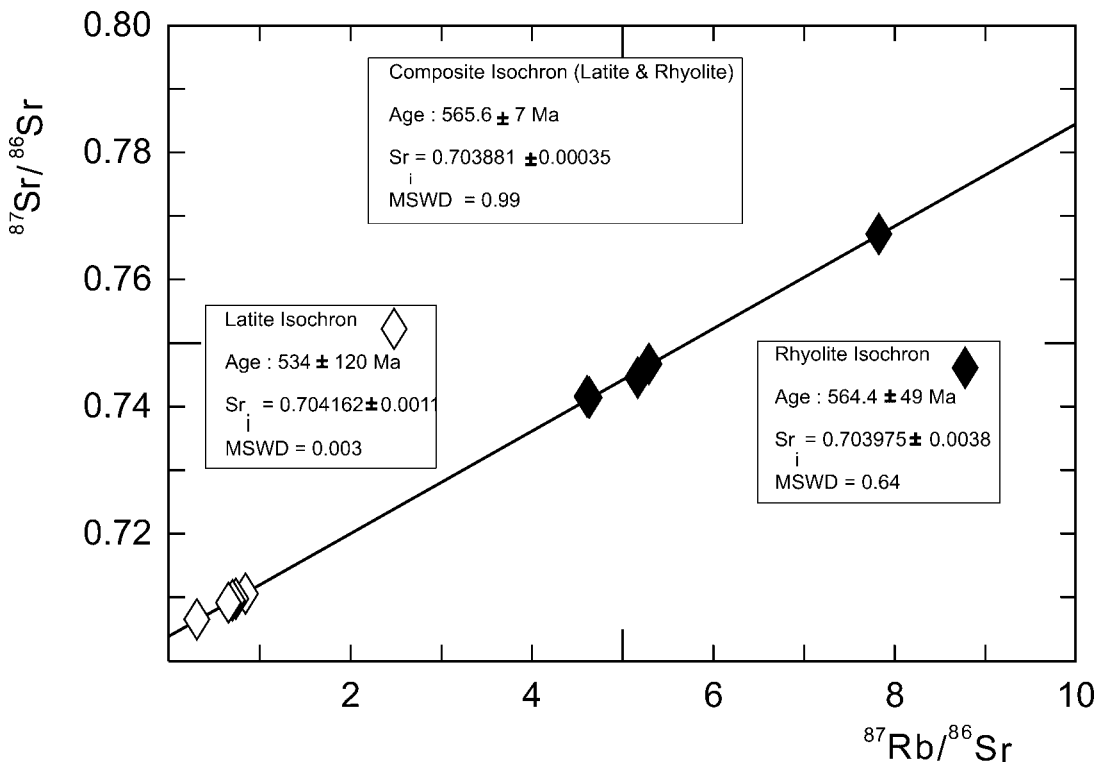

Figure 7. A Rb-Sr isochron diagram of the studied composite dikes. The separate regression lines for the latites and rhyolites are not shown. The calculations were made using the ISOPLOT plotting and regression program Version 2.96 by Ludwig (1998).

9. DISCUSSION

9.1. Petrogenesis of the rhyolite

The major element compositions of the rhyolites (e.g. high silica) can be explained either by small degrees of partial melting of a quartz-bearing mafic (granulite) source or by extreme fractional crystallization of mafic magma. The close relationship in space and time between the two rock types implies that the emplacement of the latite was rapidly followed by that of the rhyolite and that both magmas evolved in a closed magmatic system. Hence, a fractionation relationship between rhyolite and latite might be suggested; nevertheless, the following arguments render the derivation of rhyolites from latites via fractional crystallization unlikely.

- The volumetric rhyolite/latite ratio is always > 3.
- There is distinct bimodality in major and trace element distribution (Figures 2a, b, and 4).
- The binary variation plots (Figure 4, Mg versus Nb, Zr, Y, and Rb versus Sr) do not reflect a smooth decreasing relationship, which would result from fractionation of latite producing rhyolites. Other plots (e.g. Nb versus Zr, Y versus Zr) display two unrelated clusters instead of a linear trend from latites to rhyolites.
- The data points of latites exhibit a loose scatter, in contrast to the tighter scatter of rhyolites (Figure 4).
- Both rock types are characterized by different high-field strength elemental ratios (e.g. Zr/Nb, Zr/Y, Y/Nb), and other large ion lithophile elements (LILE); K/Rb ratios for the latites (270) are higher and show a wide range compared to those of the rhyolites (193) (Table 1). Ba/La ranges between 1 and 40 in latites and from 4 to 11 in rhyolites. Since these elements are highly incompatible with respect to the fractionated mineral phases, it has been argued that their ratios should not vary significantly during a closed-system fractional crystallization. Therefore, crustal contamination and/or assimilation and fractional crystallization (AFC) processes are invoked to account for the wide variation of these ratios (e.g. Davidson *et al.* 1988; Wilson *et al.* 1997). The rhyolites have narrow variation in almost all elements and elemental ratio diagrams in contrast to those of the latites.
- The latites are more enriched in light rare earth elements than the rhyolites; the $(La/Lu)_N$ values are 6.02 and 4.91 for latites and rhyolites, respectively. Moreover, the latites are higher in the REE than the rhyolites. Fractional crystallization of latites to produce rhyolites would give rise to enrichment of the REE in the rhyolites compared to the observed contents.

Guffanti *et al.* (1996) compared the heat needed for partial melting of lower basaltic crust with the heat made available from cooling and fractionation of mantle-derived basaltic magmas and established that the ratio of the produced felsic to the cooled mafic magma is about 3 to 4. Assuming that the liquidus temperatures of basaltic and felsic magmas are *c.* 1300 and *c.* 900°C, respectively, and the background temperature of the lower crust 800°C, the authors determined the degree of melting to be *c.*15%. Furthermore, it has been demonstrated that granitic melts of less than 30% melt fraction cannot leave their sources (e.g. Wickham 1987).

The lower crustal REE composition given by Taylor and McLennan (1985) was used to constrain the formation of the rhyolitic melt via modal batch melting using the formula:

$$\frac{Cl}{Co} = \frac{1}{(D + F - DF)}$$

Where *Cl* is the concentration of a trace element in the crustal melt, *Co* is the concentration of a trace element in the source rock (lower crust), *F* is the fraction of the melt (degree of partial melting), and *D* is the bulk distribution coefficient. The lower crustal mineralogy used in the calculations is: 28.6% orthopyroxene + 9.8% clinopyroxene + 5.7% K-feldspar + 54.1% plagioclase + 1.7% magnetite. The amount of melting is taken to be 30%, which is reasonable (Wickham 1987; Huppert and Sparks 1988). The latter authors discussed the role of basaltic magmas intruded into the continental crust in the generation of voluminous silicic melts. Both mafic and silicic magmas can occur in the same chamber and can mingle and mix. The granitic melt produced at the initial stages of melting was enriched in the incompatible elements and was mixed with the differentiated basaltic melt to produce the latites.

Table 3. REE data for six selected samples, together with the modelled REE data for the rhyolites, and REE data for time-equivalent rocks from adjacent areas

	Latites				Rhyolites				Jordan	Wadi Feiran		NE Desert		Lower crustal melt	10% FC	30% FC	50% FC	Di
	M1	RA2	TN1	Aver	M2	RA4	TN2	Aver	Humra granite	S1-23 Rhyolite	S1-24 Andesite	Rhyolite	Andesite					
La	30.0	31.2	47.0	36.1	52.0	21.0	25.0	32.7	22.2	20.0	49.0	n.d.	n.d.	22.2	23.6	27.1	32.7	0.4
Ce	70.0	75.3	111.5	85.6	121.0	52.1	60.0	77.7	49.2	51.0	113.0	68.9	48.0	48.3	51.1	58.4	69.7	0.5
Nd	43.0	43.6	59.2	48.6	50.9	29.5	32.1	37.5	19.4	16.0	55.0	29.4	25.3	24.9	25.4	26.5	28.0	0.8
Sm	10.2	12.8	16.4	13.1	13.0	9.1	9.0	10.3	5.8	3.0	12.0	5.3	5.4	6.0	6.1	6.5	7.0	0.8
Eu	2.3	2.3	2.3	2.3	0.0	0.2	0.3	0.2	0.4	0.4	2.4	1.0	1.5	0.9	0.7	0.4	0.2	3.0
Gd	9.3	9.6	10.4	9.8	8.4	8.0	7.7	8.0	2.6	2.1	8.2	4.1	4.9	5.8	5.9	6.1	6.3	0.9
Tb	1.8	1.9	2.0	1.9	1.9	2.3	2.1	2.1	0.5	0.0	0.0	0.0	0.0	0.0	0.0	0.0	0.0	0.0
Dy	7.7	8.1	7.7	7.8	6.8	8.1	8.1	7.6	3.3	2.1	7.9	3.6	4.0	6.5	6.5	6.5	6.5	1.0
Ho	1.4	1.1	1.4	1.3	0.0	1.6	1.4	1.5	1.3	0.4	1.5	0.0	0.0	0.0	0.0	0.0	0.0	0.0
Er	4.1	4.1	3.1	3.7	2.0	3.6	4.0	3.2	1.9	1.3	4.2	2.1	2.0	3.8	3.9	3.9	4.0	0.9
Tm	0.5	0.4	0.5	0.5	0.5	0.6	0.5	0.5	0.3	0.0	0.0	0.0	0.0	0.0	0.0	0.0	0.0	0.0
Yb	3.8	4.0	3.7	3.8	3.6	4.9	4.5	4.3	2.1	1.3	3.6	2.1	1.9	3.7	3.7	3.9	4.2	0.8
Lu	0.6	0.6	0.6	0.6	0.6	0.8	0.7	0.7	0.4	0.0	0.0	0.0	0.0	0.5	0.5	0.5	0.5	0.7
ΣREE	185	195	266	215	261	142	155	186	109	75	233	177	93	122	127	140	159	
$(La/Lu)_N$	4.94	4.97	8.27	6.02	9.14	2.78	3.7	4.91	6.48	10.2	8.98	8.35	6.59	4.79	5.02	5.53	6.3	
Eu/Eu*	0.8	0.72	0.67	0.73	0.009	0.08	0.13	0.02	0.4	0.4	0.67	0.95	0.8	0.53	0.11	0.2	0.35	

FC, fractional crystallization; Di, bulk distribution coefficient calculated for the fractionating assemblage (hornblende, biotite, alkali feldspars and quartz).

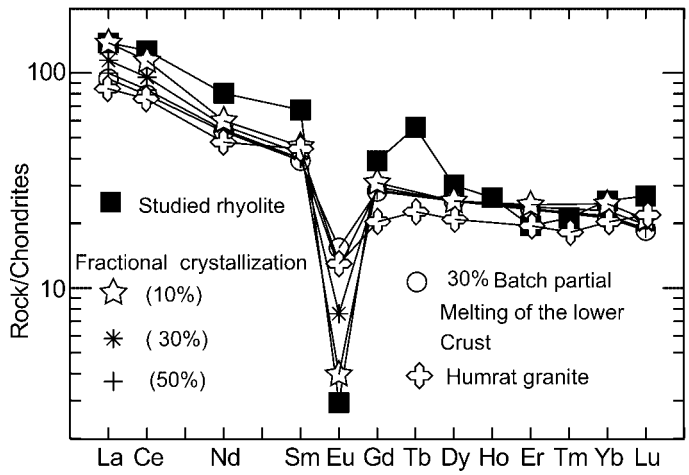

Figure 8. REE chondrite-normalized plot for average studied rhyolite, the modelled rhyolitic melt, and the Humrat granite from SW Jordan.

By contrast, the rhyolitic melt batch, which was able to leave its place of formation and form the core of the composite dikes, suffered extensive fractional crystallization. As it has been demonstrated on the basis of mineral vectors (Figure 4), the interelemental variation in the rhyolite can be best explained by 30 to 50% fractionation of hornblende, biotite, feldspar and quartz. To constrain the degree of fractionation quantitatively, modelling of REE elements using the equation of Arth (1976) was applied. The calculations were carried out using the REE values (C_0) of the 30% partial melt of the lower crust (Table 3) and the crystal assemblage of 15% hornblende + 5% biotite + 30% plagioclase + 30% K-feldspar + 20% quartz. The percentages of the fractionating phases are assumed based on the petrography and the vector diagrams (Figure 4). The bulk distribution coefficients were calculated for (mineral/felsic melt) using the compilation of *Kd*'s given by Rollinson (1993). The amount of fractional crystallization was set at 10, 30, and 50%, respectively. The modelled REE concentrations are plotted together with the average rhyolites (Figure 8). The average rhyolite composition best fits the 50% fractionation pattern.

9.2. Petrogenesis of the latite

The most primitive latite represented by the sample RA3 (cf. Mg # = 0.52; Table 1), which has the highest concentrations (in ppm) of compatible elements (Cr = 26, Ni = 16, Sc = 22, and V = 191) among the whole mafic end member of the composite dikes. Yet, this sample is far away from being considered primary mafic magma, which would have existed in equilibrium with a mantle source region. According to Clague and Frey (1982), the accepted criteria for primary basaltic magma are Mg # > 65 and Ni contents > 235 ppm. The Ghuweir mafics in Feinan area (see age relationships) represent a shallowly intruded stock containing rocks closely matching these criteria (i.e. GW23; Mg # 61; Ni = 185 ppm). Because the age of these mafics coincides with the age of the composite dikes within analytical uncertainty, we consider the primitive samples of these mafics as a candidate parent for the latites. The most primitive latite (RA3; Mg # 52) can be derived from GW23 (Mg # 61) by fractional crystallization of olivine, plagioclase, pyroxene, and magnetite in a ratio of 9:30:20:6. This fractionated mineral assemblage comprises about 65% of the original magma. Least square mass-balance calculations of major elements using the XLFRAC program (Stormer and Nicholls 1978) were utilized for the modelling ($r^2 = 1.15$; sums of squares of residuals). The same program was applied to model the chemical variation within the investigated latites. The samples RA3 and GT4 were selected as the most primitive and the most differentiated samples, respectively. Sums of squares of residuals of less than 2 were obtained only when the plagioclase, amphibole and/or pyroxene were removed and appreciable amounts of alkali feldspar and quartz were added. This lends support to the mineral vector modelling of fractional crystallization, which could not explain the trace element variation on its own, suggesting involvement of another mechanism. The mechanism in this case is mixing with a granitic melt that

is highly enriched in elements such as LILE (e.g. Ba, Rb), in particular products of the initial stages of partial melting.

The Sr isotopic data of the investigated dikes are used to constrain, at least qualitatively, the role of mixing and AFC processes in the evolution of the latites. Provided that mixing is the only process involved in the genesis of a magmatic suite and that the members are compositionally homogeneous, the isotopic data on the Sr versus $^{87}Sr/^{86}Sr$ and the 1/Sr versus $^{87}Sr/^{86}Sr$ diagrams should define a hyperbolic mixing curve and a straight line, respectively (Langmuir *et al.* 1978). The latite data do not fulfil this requirement (Figure 9); this, together with the geochemical arguments listed above, warrants the involvement of another mechanism in their genesis. Their chemical characteristics provide evidence of both fractional crystallization and crustal assimilation processes (Allègre and Minster 1978; DePaolo 1981). Using the DePaolo's equations (1981) with the Ghuweir Mafics as a starting material and the rhyolite as a contaminant, several calculations were performed of the Sr isotopes. The results along with the isotopic data for the composite dikes are plotted on the Sr versus $^{87}Sr/^{86}Sr$ diagram (Figure 9; DePaolo 1981). R (the assimilation rate/crystallization rate) was taken as 0.75 while the D^{Sr} (bulk distribution coefficient for Sr between the fractionating minerals and the magma) varied between 0.6 and 2. The plot demonstrates convincingly that the latites are not the result of simple mixing of a crustal melt and a mantle-derived melt but rather the result of both mixing and fractional crystallization, because these samples fall on trajectories defined by the different D^{Sr} values. The changes in the D^{Sr} reflect varying amounts of plagioclase in the fractionating assemblage.

On the basis of the previous discussion, we interpret the genesis of the latite as evolving by differentiation of a parental mantle magma concurrent with a substantial proportion of crustal assimilation and/or mixing with granitic melt formed as a result of the intrusion of basaltic magma into the lower crust. However, the rhyolitic magma is exclusively of anatectic origin in the lower continental crust.

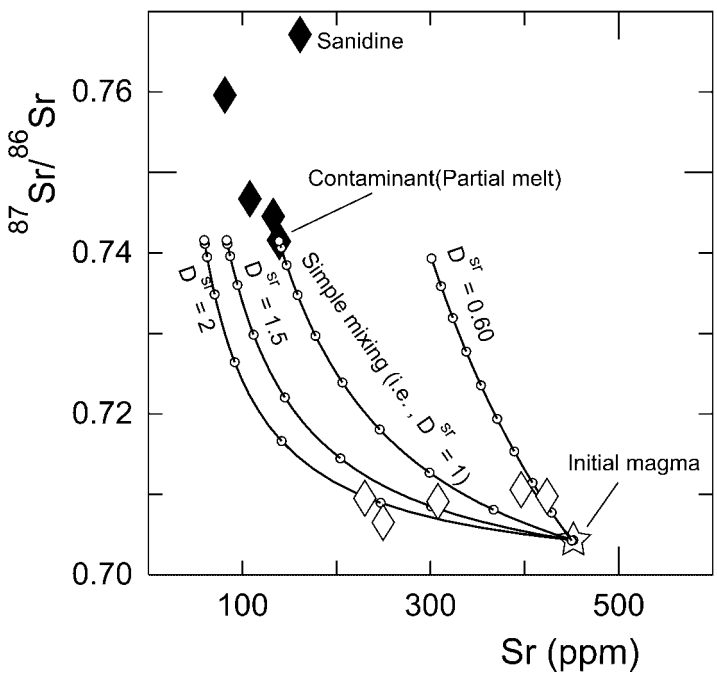

Figure 9. $^{87}Sr/^{86}Sr$ versus Sr plot (DePaolo 1981) for the investigated rocks. D^{Sr} is the bulk distribution coefficient for Sr between the fractionating minerals and the magma. A basaltic trachyandesite from the Ghuweir Mafics (Feinan; Figure 1) has been selected as representative of the initial magma from which the latites might have derived (GW-21; Rb = 14.8 ppm, Sr = 451.9 ppm, $^{87}Sr/^{86}Sr = 0.7042$); GT-7 (Table 2) has been selected as representative of the rhyolite contaminant (partial melt). Their assimilation rate/crystallization rate was taken as 0.75.

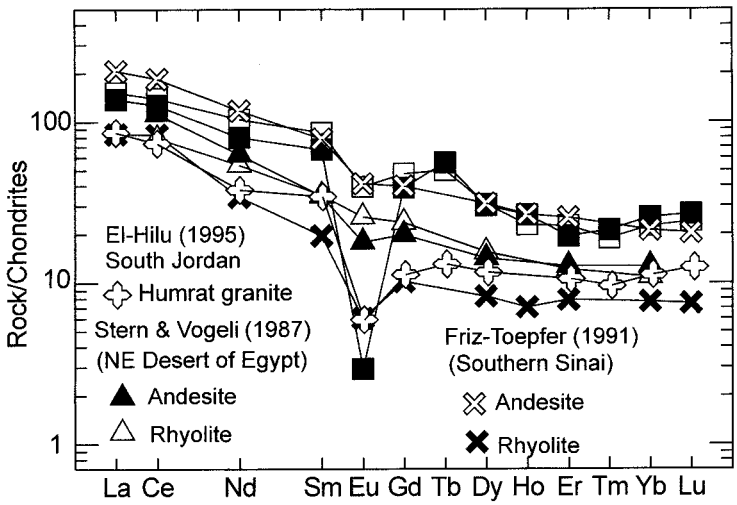

Figure 10. REE chondrite-normalized plots for mean studied rhyolite and latite compared with time-equivalent rocks from adjacent areas.

9.3. Regional correlation

The REE data for average rhyolites and latites are plotted together with relevant data on time equivalent composite dikes (Figure 10) from southern Sinai (Friz-Töpfer 1991), from the North East Desert of Egypt (Stern and Voegeli 1987), and Humrat granite from SW Jordan (El-Hilu 1995). The similarity in the slopes of the REE patterns at variable ΣREE suggest similar origins for these rocks but different degrees of fractional crystallization.

9.4. Composite dikes formation model

On the basis of the above-mentioned discussion we suggest the following model for the formation of the composite dikes, which is summarized in Figure 11.

I. Extension of the overthickened Pan-African crust followed by decompressive partial melting of the upper mantle; the intrusion and fractional crystallization of the mafic melt in the lower crust provided the thermal input needed to initiate partial melting of the lower crust. The fractionated mafic magma mixed with the initial batches of the rhyolitic melt to form the latites.
II. Fractional crystallization of the mantle-derived magma and continued magma mixing, with partial melts up to 30%, gave rise to a zoned magma chamber. By virtue of its high viscosity and its high phenocryst contents (30–40%), the rhyolite magma was less mobile than the latite magma. The viscosity dependence of dike nucleation promotes dikes to originate first from the lower more mafic sections of the stratified chambers due to the great viscosity contrasts within these chambers (McLeod and Tait 1999).
III. The less viscous latite magma filled induced-extension fractures and solidified. Median fractures developed within still hot (supported by the lack of chilled margins of rhyolite against latite) latite dikes.
IV. The highly viscous, conspicuously porphyritic rhyolite magma intruded into the median fractures in the latite to produce very symmetrical composite dikes.

10. CONCLUSIONS

The following conclusions can be drawn from this study.

1. The investigated composite dikes comprise a thick rhyolite core, symmetrically flanked by relatively thin latite rims, which form on average one-quarter of the composite dike thickness.

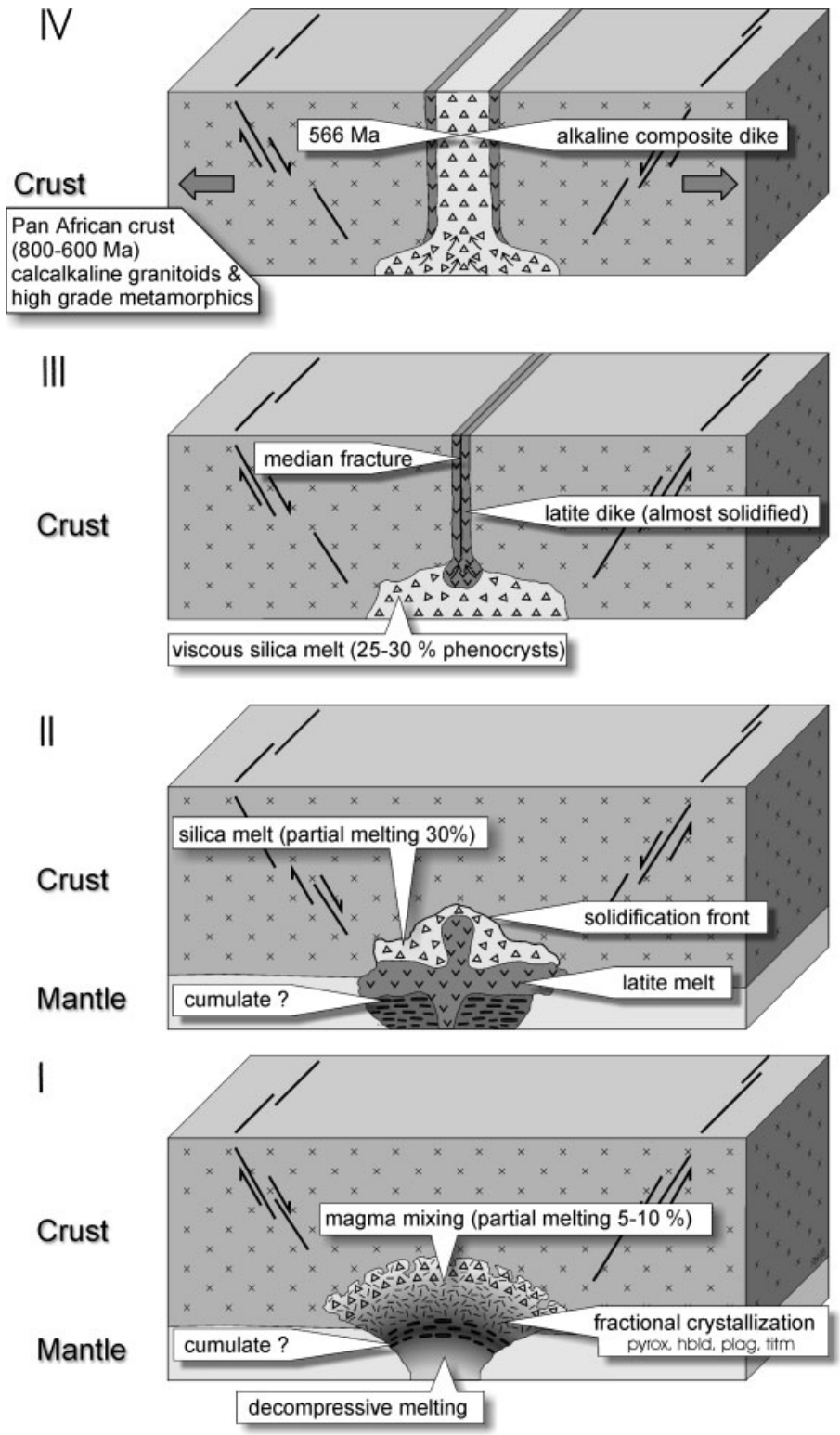

Figure 11. A cartoon of the tectonomagmatic evolution of the investigated composite dikes.

2. The Rb-Sr whole-rock composite isochron of ten data points gave an age of 565 ± 7 Ma and an initial ratio of 0.703881 ± 0.00035 (MSWD $= 0.99$). Age relationships of the host rocks indicate that this age is appropriate.
3. The geochemical data of the latite and rhyolite are not in favour of a fractional crystallization relationship between the two end members of the composite dike.
4. The geochemical features of the latites are best explained by assimilation–fractional crystallization processes (DePaolo 1981) where a lower-crustal granitic melt represents the assimilant (contaminant).
5. The rhyolites have the chemical features diagnostic of A-type magmas and were formed by 30% batch melting of the lower crust, which was induced by thermal energy supplied by the mantle-derived latite magma.
6. The emplacement of the composite dikes took place in an extensional post-collisional tectonic regime.

ACKNOWLEDGEMENTS

The Deutsche Akademische Austauschdienst (DAAD) supported the research stay of the first author in Germany. The sabbatical leave offered by the University of Jordan to the first author is highly appreciated. The analysis costs and stay expenses were covered partially by a grant from the Higher Council of Science and Technology of Jordan. Reviews by W. Frisch and an anonymous referee substantially improved the manuscript and are highly appreciated. R. J. Stern, University of Texas at Dallas kindly improved the English of this paper. We would like to thank Dipl.-Geol. Ralf Hollaender for the preparation of some of the diagrams.

REFERENCES

Abdullah N. 1989. *Geology, geochemistry and petrology of the Precambrian rocks of Wadi Rahma, Wadi Araba, SW Jordan.* MSc Thesis, University of Jordan, Amman, Jordan.

Akaad MK, Noweir AM. 1980. Geology and lithostratigraphy of the Arabian Desert orogenic belt of Egypt between latitudes 25° 35′ and 26° 30′ N. In *Evolution and Mineralization of the Arabian-Nubian Shield*, Coaray PG, Tahoun (eds). Bulletin 3. Institute of Applied Geology: Jeddah; 127–135.

Allègre CJ, Minster JF. 1978. Quantitative models of trace elements behaviour in magmatic processes. *Earth and Planetary Science Letters* **38**: 1–25.

Arth JG. 1976. Behaviour of trace elements during magmatic processes—a summary of theoretical models and their applications. *Journal of Research of the Geological Survey of America* **4**: 41–47.

Bender F. 1974. Explanatory notes on the geological map of the Wadi Araba, Jordan: Scale 1:100.000; 3 sheets. *Geologisches Jahrbuch* **B10**: 3–62.

Bender JF, Hanson GF, Bence AE. 1982. The Cortlandt Complex: evidence for large-scale immiscibility involving granodiorite and dioritic magmas. *Earth and Planetary Science Letters* **58**: 122–140.

Beyth M, Heimann A. 1999. The youngest igneous event in the crystalline basement of the Arabian-Nubian Shield, Timna Igneous Complex. *Israel Journal of Earth Science* **48**: 113–120.

Beyth M, Stern RJ, Altherr R, Kröner A. 1994. The late Precambrian Timna igneous complex, Southern Israel: evidence for comagmatic-type sanukitoid monzodiorite and alkali granite magma. *Lithos* **31**: 103–124.

Blaxland A, Gohn E, Hack U, Hoffer E. 1979. Rb-Sr ages of the late tectonic granites in the Damara orogen, SW Africa, Namibia. *Neues Jahrbuch für Mineralogie, Monatshefte* **11**: 498–508.

Brook M, Ibrahim KH, McCourt W. 1990. New geochronological data from the Arabian Shield area of SW Jordan. *Proceedings of the Third Jordanian Geological Conference*, Amman; 361–394.

Clague DA, Frey FA. 1982. Petrology and trace elements geochemistry of the Honolulu volcanics, Oahu: implications for oceanic mantle beneath Hawaii. *Journal of Petrology* **23**: 447–504.

Creaser RA, Price RC, Wormald RJ. 1991. A-type granites revisited: assessment of residual-source model. *Geology* **19**: 163–166.

Cribb JW, Barton M. 1996. Geochemical effects of decoupled fractional crystallization and crustal contamination. *Lithos* **37**: 293–307.

Davidson JP, Duncan MA, Ferguson KM, Colucci MT. 1988. Crust-magma interactions and the evolution of arc magmas: the San Pedro-Pellardo Volcanic complex, southern Chilean Andes. *Geology* **15**: 443–446.

DePaolo DJ. 1981. Trace element and isotopic effects of combined wall rock assimilation and fractional crystallization. *Earth and Planetary Science Letters* **53**: 189–202.

Dewey JF. 1988. Extensional collapse of the orogens. *Tectonics* **7**: 1123–1139.

Eby NG. 1992. Chemical subdivision of the A-type granitoids: petrogenetic and tectonic implications. *Geology* **20**: 641–644.

El-Hilu MM. 1995. *Mineralogy, geochemistry and petrogenesis of the Humrat granite in the area of Quweira, south Jordan.* MSc Thesis, University of Jordan, Amman, Jordan.

Förster H-J, Tischendorf G, Trumbull RB. 1997. An evaluation of the Rb vs. (Y + Nb) discrimination diagram to infer tectonic setting of silicic igneous rocks. *Lithos* **40**: 261–293.
Frisch W, Abdel-Rahman AM. 1999. Petrogenesis of the Wadi Dib alkaline ring complex, Eastern Desert of Egypt. *Mineralogy and Petrology* **65**: 249–275.
Friz-Töpfer A. 1991. Geochemical characterisation of Pan-African dyke swarms in southern Sinai: from continental margin to intraplate magmatism. *Precambrian Research* **49**: 281–300.
Garfunkel Z. 1999. History and paleogeography during the Pan-African orogen to stable platform transition: reappraisal of the evidence from the Elat area and the northern Arabian-Nubian Shield. *Israel Journal of Earth Science* **48**: 135–157.
Greiling RO, Abdeen MM, Dardir AA, Al-Akhal H, EL-Ramly MF, Kamal-El Din GM, Osman AF, Rashwan AA, Rice AA, Sadek MF. 1994. A structural synthesis of the Proterozoic Arabian-Nubian Shield in Egypt. *Geologische Rundschau* **83**: 484–501.
Grove TL, Donnelly-Nolan JM. 1986. The evolution of young silicic lavas at the Medicine Lake Volcano, California: implications for the origin of compositional gaps in calc-alkaline series lavas. *Contributions to Mineralogy and Petrology* **92**: 281–302.
Guffanti M, Clynne MA, Muffler LJP. 1996. Thermal and mass implications of magmatic evolution in the Lassen volcanic region, California and constraints on basalt influx to the lower crust. *Journal of Geophysical Research* **101**: 3001–3013.
Huppert HE, Sparks RSJ. 1988. The generation of granitic magmas by intrusion of basalt into continental crust. *Journal of Petrology* **29**: 599–624.
Ibrahim KM, McCourt WJ. 1995. Neoproterozoic granitic magmatism and tectonic evolution of the northern Arabian Shield: evidence from Southwest Jordan. *Journal of African Earth Sciences* **20**: 103–118.
Irvine NT, Baragar WRA. 1971. A guide to the geochemical classification of the common volcanic rocks. *Canadian Journal of Earth Sciences* **8**: 523–548.
Jarrar G. 1985. Late Proterozoic crustal evolution of the Arabian–Nubian shield in the Wadi Araba area, SW-Jordan. *Geologisches Jahrbuch* **B61**: 3–87.
Jarrar G. 1992. Geochemistry and petrogenesis of an alkali-feldspar rhyolite suite from Wadi Museimir, Central Wadi Araba, Jordan. *Chemie der Erde* **52**: 301–312.
Jarrar G. 1998. Mineral chemistry in dioritic hornblendites from Wadi Araba, SW Jordan. *Journal of African Earth Sciences* **26**: 285–295.
Jarrar G. 2001. The Youngest Neoproterozoic Mafic Dike Suite in the Arabian Shield; mildly alkaline dolerites from South Jordan-their geochemistry and petrogenesis. *Geological Magazine* **138**: 309–323.
Jarrar G, Wachendorf H, Zellmer H. 1991. The Saramuj Conglomerate: evolution of a Pan-African molasse sequence from southwest Jordan. *Neues Jahrbuch für Geologie und Paläontologie, Monatheft* **H6**: 335–356.
Jarrar G, Wachendorf H, Saffarini G. 1992. A late Proterozoic bimodal volcanic/subvolcanic suite from Wadi Araba, Southwest Jordan. *Precambrian Research* **56**: 51–72.
Jarrar G, Wachendorf H, Zachmann D. 1993. A Pan-African pluton intruding the Saramuj Conglomerate, South-west Jordan. *Geologische Rundschau* **82**: 121–135.
Jarrar G, Manton W, Stern RJ. In press. Late Neoproterozoic A-type granites in the Northernmost Arabian-Nubian Shield formed by fractional crystallization of basaltic melts. *International Journal of Earth Science*.
Kessel R, Stein M, Navon O. 1998. Petrogenesis of Late Neoproterozoic dikes in the northern Arabian-Nubian Shield: implications for the origin of A-type granites. *Precambrian Research* **92**: 195–213.
Koyaguchi T, Kaneko K. 1999. A two-stage thermal evolution model of magmas in continental crust. *Journal of Petrology* **40**: 241–234.
Kröner A. 1984. Late Precambrian plate tectonics and orogeny: a need to redefine the term Pan-African. In *African Geology*, Klerks J, Michot J (eds). Musée royal de l'Afrique centrale: Tervuren; 23–26.
Landenberger B, Collins WJ. 1996. Derivation of A-type granites from dehydrated charnockitic lower crust: evidence from the Chaelundi complex, eastern Australia. *Journal of Petrology* **37**: 145–170.
Langmuir CH, Vocke DR, Gilbert H. 1978. A general mixing equation with applications to icelandic basalts. *Earth and Planetary Science Letters* **37**: 380–392.
Le Bas MJ, Le Maitre RW, Streckeisen A, Zanettin B. 1986. A chemical classification of volcanic rocks based on the total alkali-silica diagram. *Journal of Petrology* **27**: 745–750.
Ludwig KR. 1998. *ISOPLOT: A plotting and regression program for radiogenic isotope data. Version 2.96*. United States Geological Survey Open-File Report 91–445.
McLeod P, Tait S. 1999. The growth of dikes from magma chambers. *Journal of Volcanology and Geothermal Research* **92**: 231–245.
Meen JK. 1990. Elevation of potassium content of basaltic magma by fractional crystallization: the effect of pressure. *Contributions to Mineralogy and Petrology* **104**: 309–331.
Pearce JA. 1980. Geochemical evidence for the genesis and eruptive setting of lavas from Tethyan ophiolites. *Proceeding of the International Ophiolite Symposium*, Cyprus 1979. Institute of Mining and Metallurgy: 261–272.
Pearce JA. 1996. Sources and settings of granitic rocks. *Episodes* **19**: 120–125.
Pearce JA, Norry MJ. 1979. Petrogenetic implications of Ti, Zr, Y, and Nb variations in volcanic rocks. *Contributions to Mineralogy and Petrology* **69**: 33–47.
Pearce JA, Harris NB, Tindle AG. 1984. Trace elements discrimination diagrams for the tectonic interpretation of granitic rocks. *Journal of Petrology* **25**: 956–983.
Peccerillo R, Taylor SR. 1976. Geochemistry of Eocene calc-alkaline volcanic rocks from the Kastamonu area, northern Turkey. *Contribution to Mineralogy and Petrology* **58**: 63–81.
Pudlo D, Franz G. 1994. Dike rock generation and magma interactions in the Bir Safsaf igneous complex, SW Egypt: implications for the Pan-African evolution in North East Africa. *Geologische Rundschau* **83**: 523–536.
Rollinson H. 1993. *Using geochemical data: evaluation, presentation, interpretation*. Longman: Harlow.
Sha'ban KH. 1996. *Rahma Synplutonic diorite dikes: Geology, petrography and geochemistry.* MSc Thesis, University of Jordan, Amman, Jordan.

Snyder D, Crambes CH, Tait S, Wiebe RA. 1997. Magma mingling in dikes and sills. *Journal of Geology* **105**: 75–86.
Steiger RH, Jäger E. 1977. Subcommission on geochronology: convention on the use of decay constants in geochronology and cosmochronology. *Earth and Planetary Sciences Letters* **36**: 359–362.
Stern RJ, Manton WJ. 1987. Age of Feiran basement rocks, Sinai: implications for late Precambrian crustal evolution in the northern Arabian-Nubian Shield. *Journal of the Geological Society, London* **144**: 569–575.
Stern JR, Voegeli DA. 1987. Geochemistry, geochronology, and petrogenesis of a late Precambrian (590 Ma) composite dike from the North Eastern Desert of Egypt. *Geologische Rundschau* **76**: 325–341.
Stormer JC Jr, Nicholls J. 1978. *XLFRAC:* a program for the interactive testing of magmatic differentiation models. *Computers & Geosciences* **4**: 143–159.
Taylor SR, McLennan SM. 1985. *The Continental Crust: Its composition and evolution.* Blackwell: Oxford.
Turner SP, Foden JD, Morrison RS. 1992. Derivation of some A-type magmas by fractionation of basaltic magma: an example from the Padthaway Ridge, South Australia. *Lithos* **28**: 151–179.
Wachendor H, Jarrar G, Zachmann D. 1985. The role of pressure in control of potassium, sodium, and copper concentration in hypabyssal intrusives as documented in late Precambrian dikes in SW Jordan. *Precambrian Research* **30**: 221–248.
Whalen JB, Currie KL, Chappell BW. 1987. A-type granites: Geochemical characteristics, discrimination and petrogenesis. *Contributions to Mineralogy and Petrology* **95**: 407–419.
White AJR, Collins WJ, Chappell BW. 1982. Influence of melt structure on the trace element composition of granites. In *Geology of Granites and their Metallogenetic Relations*, Kegin Xu, Guangchi Tu (eds). Proceedings of International Symposium, Nanjing University, China: 737–751.
Wickham SM. 1987. The segregation and emplacement of granitic magmas. *Journal of the Geological Society* **144**: 281–297.
Wiebe RA, Ulrich R. 1997. Origin of composite dikes in the Gouldsboro granite, coastal Maine. *Lithos* **40**: 157–178.
Willis KM, Stern RJ, Clauer N. 1988. Age and geochemistry of late Precambrian sediments of the Hammamat Series from the NE Desert of Egypt. *Precambrian Research* **42**: 173–187.
Wilson M, Tankut A, Guleçn N. 1997. Tertiary volcanism of the Galatia province, north-west central Anatolia, Turkey. *Lithos* **42**: 105–121.
Winchester JA, Floyd PA. 1977. Geochemical discrimination of different magma series and their differentiation products using immobile elements. *Chemical Geology* **20**: 325–343.
Wood DA, Joron JL, Treuil M, Norry M, Tarney J. 1979. Elemental and Sr isotope variations in basic lavas from Iceland and the surrounding ocean floor. *Contributions to Mineralogy and Petrology* **70**: 319–339.
Zachmann DW. 1988. Matrix effects in the separation of Rare-Earth Elements, scandium, and yttirium and their determination by inductively coupled plasma optical emssion spectroscopy. *Analytical Chemistry* **60**: 420–427.

Scientific editing by George Rowbotham.

